Title

Reversible Anionic Redox Activities in Conventional LiNi1/3Co1/3Mn1/3O2 Cathodes

Journal

Angewandte Chemie International Edition, 59(22)

ISSN

1433-7851

Authors

Lee, Gi-Hyeok

Wu, Jinpeng

Kim, Duho

et al.

Publication Date

2020-05-25

DOI

10.1002/anie.202001349

Peer reviewed

Reversible Anionic Redox Activities in Conventional $LiNi_{1/3}Co_{1/3}Mn_{1/3}O_2$ Cathodes

Gi-Hyeok Lee[†], Jinpeng Wu[†], Duho Kim, Kyeongjae Cho, Maenghyo Cho, Wanli Yang* & Yong-Mook Kang*

Communications **Abstract:** The redox reaction of oxygen has been considered critical in controlling the electrochemical properties of Li-excessive layered oxide electrodes. However, conventional electrode materials without over-lithiation remain the most practical if their performance could be improved through rational approaches. Typically, cationic redox reactions are believed to dominate the electrochemical operations in conventional electrodes, and the involvement of anionic redox reactions, although proposed, is yet to be clarified through reliable characterizations. Here, we show unambiguous evidence of reversible anionic redox reactions in $LiNi_{1/3}Co_{1/3}Mn_{1/3}O_2$., with a detailed quantification on its reversibility upon electrochemical cycling. Two types of oxygen involvements are discussed. One is the typical involvement of O through hybridization with transition metals throughout the electrochemical operation; the other is the intrinsic O redox at high potentials, which is 75% reversible during initial cycling and 63% retained after 10 cycles. Our results clarify the reaction mechanism at high potentials in conventional layered electrodes involving both cationic and anionic reactions. ~~More importantly~~Additionally, our combined characterizations ~~reveals~~ indicate a critical role of transition-metals for oxygen redox activities and the optimism of utilizing reversible oxygen redox reactions ~~is promising~~ in conventional layered oxides for high-capacity lithium-ion batteries.

[*] Prof. Y.-M. Kang
Department of Materials Science and Engineering
Korea University
Seoul 02841, Republic of Korea
dake1234@korea.ac.kr
Dr. W. Yang, Dr. J. Wu
Advanced Light Source
Lawrence Berkeley National Laboratory
Berkeley, California 94720, United States
wlyang@lbl.gov
G.-H. Lee
Department of Energy and Materials Engineering
Dongguk University-Seoul
Seoul 04620, Republic of Korea
Dr. J. Wu
Geballe Laboratory for Advanced Materials
Stanford University
Stanford, California 94305, United States
Prof. D. Kim
Department of Mechanical Engineering
Kyung Hee University
Yongin 17104, Republic of Korea
Prof. K. Cho
Department of Materials Science and Engineering and
Department of Physics
University of Texas at Dallas
Richardson, Texas 75080, United States
Prof. M. Cho
Institute of Advanced Machines and Design
Seoul National University
Seoul 08826, Republic of Korea

[†]G.-H. Lee and J. Wu contributed equally to this work.

Supporting information for this article is given via a link at the end of the document.

Introduction

Rapid increases in the need for mobile electronic devices and large-scale energy storage applications have now created a strong demand for the cathode materials with higher energy densities in lithium-ion batteries (LIBs).[1] Among various cathode candidates, layered oxides have been regarded as the most intriguing materials compared to the other cathode materials owing to the higher capacities and more possibilities for the extended charging voltages. However, electrochemical cycling of layered compounds often cannot reach their theoretical limit without compromising the stability and cyclability. For example, $LiCoO_2$, although widely used commercially, has a practical capacity of only about half of its theoretical value because of the structural instability with extended lithium extraction.[2] In this regard, to improve the reversible capacity and structural stability simultaneously, Ni-based layered oxides ($LiNi_{1-x-y}Co_xMn_yO_2$) have been extensively studied for not only fundamental purpose but also its commercialization because $LiNi_{1-x-y}Co_xMn_yO_2$ is expected to benefit from Ni on its capacity and Mn on its stability.[3] ~~Nonetheless, o~~Operating such conventional layered materials at high potentials towards their theoretical capacity has been a critical practice to release the full benefits of layered compounds for high-capacity high-power battery electrodes.

During the battery operation at high potentials, the involvement and control of oxygen ~~have~~ become a critical issue for realizing the high-voltage cycling while maintaining stability. The proposed anionic redox reaction has recently attracted considerable attention due to its potential to improve the energy density of battery cathode materials.[4] **Most studies of the anionic redox reactions have focused on Li-excess layered compounds, which indeed displays high capacity beyond their cationic redox reactions ($M^{n+}/M^{(n+1)+}$), however, suffer extensive stability issues that remain inevitable so far.**[5] Therefore, extending the oxygen redox concept into the non-

~~overlithiated~~ Li-rich compounds for improved and stable capacity becomes ~~remains as an elusive but a~~ **critical challenge,** especially **considering that all commercially viable materials so far are based on such conventional compounds.**

~~Previous s~~**Studies of conventional materials** before the establishment of oxygen redox concept **often did not differentiate the dedicated oxygen redox reactions from the transition-metal (TM)-O hybridization effects** in the material, e.g., ~~. For example, the investigations on both the oxygen and Co in~~ $LiCoO_2$ ~~indicated that oxygen could get involved in the redox reactions mainly through the hybridization with Co~~.[6] ~~Indeed, m~~Most of the explorations on conventional NCM layered oxides have been

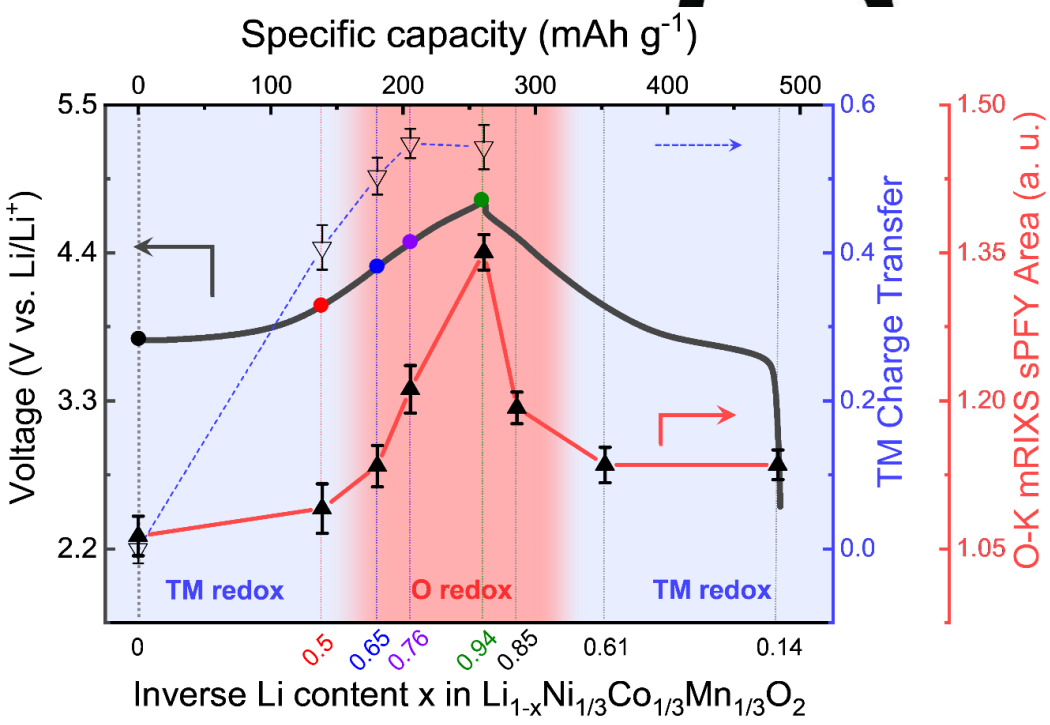

Figure 1. Electrochemical profile and corresponding TM/O redox behaviors of $LiNi_{1/3}Co_{1/3}Mn_{1/3}O_2$. An initial galvanostatic curve of $LiNi_{1/3}Co_{1/3}Mn_{1/3}O_2$ (dark grey curve using left Y-axis) obtained up to 4.8 V vs. Li/Li^+ with a constant current density of 20 mA g^{-1} at room temperature, plotted as functions of both specific capacity and delithiation level Li content (x). The electron charge transfer from TM redox during charging (blue dashed line) is quantified from soft X-ray spectroscopy and indicates the TM redox contributions only at low voltage region. The O-*K* mRIXS-sPFY area (red line) represents the intensity of the oxidized oxygen feature, which suggests that O redox takes place at high voltage region and is about 75% reversible during the initial cycle. Quantifications are performed based on independent TM and O experiments with results discussed in Figure 2 and 3, and the Table S2 includes the detailed value.

focusing on the cationic redox reactions (Ni^{2+}/Ni^{4+} and Co^{3+}/Co^{4+}) with only general discussions on the involvements of oxygen through the TM-O hybridization.[7] While there is no doubt that the TM-O hybridization is critical in battery operations with oxygen redox contributions, today's concept of lattice oxygen redox refer to a dedicated oxygen contribution and are intrinsically different from the involvement of oxygen based on TM-O hybridization.[4h, 4j] ~~Besides, oxygen redox reactions have been reported in Mg-doped Na-ion battery cathodes without excess Na; however, one should note that the bonding between Mg and O is fundamentally different from conventional 3d TM systems and resembles that of Alkali elements.[8] Therefore, these findings do not represent the electronic configurations in conventional 3d TM based non-overlithiated layered cathodes.~~ A complete picture of the involvement of oxygen and the clarification of dedicated lattice oxygen redox reactions in the conventional NCM cathodes ~~become~~ is thus critical for innovating and improving commercially viable materials based on non-overlithiated 3d TM oxides.

Herein, we provide a comprehensive analysis of the redox mechanism of both the cationic and anionic activities in $LiNi_{1/3}Co_{1/3}Mn_{1/3}O_2$ across a wide range of potential with the focus on the oxygen activities at high potentials. As discussed in details later in the manuscript, ~~We~~ we distinguished two different types of O activities: the TM-O hybridization ~~evolvement, which is affected by both TM and O redox~~ throughout the whole electrochemical cycling, and the intrinsic lattice O redox reactions only at high potentials. Our experimental evidence unambiguously reveals the lattice O redox in the conventional NCM cathode at the high electrochemical potential region, which has~~and more importantly, the lattice oxygen redox reactions are~~ about 75% reversibil~~ity~~le during the initial cycle with more than half of the amount retained after 10 cycles.

Through a series of hard and soft X-ray spectroscopy, we clarify the complete picture of the redox mechanism of such conventional NCM materials involving i) TM redox activities at relatively low potentials; ii) TM-O hybridization throughout the whole electrochemical range, and iii) dedicated oxygen redox reactions at high potentials above ~2/3 delithiation level. Note again that the identification and understanding of O activities are vital for utilizing the full potential of conventional cathode materials, and our results provide ~~the most~~ direct evidence~~support~~ of the optimism on utilizing lattice oxygen redox in non-overlithiated layered compounds towards commercially viable electrodes with high capacity and energy density.

Results and Discussion

General electrochemical behaviors

Before presenting our detailed experimental detections of the TM and oxygen redox chemistry, we first define a general electrochemical range upon the cycling profile of NCM used in this work. Figure 1 shows the initial charge curve of $LiNi_{1/3}Co_{1/3}Mn_{1/3}O_2$ (NCM) obtained up to 4.8 V vs. Li/Li^+ (see

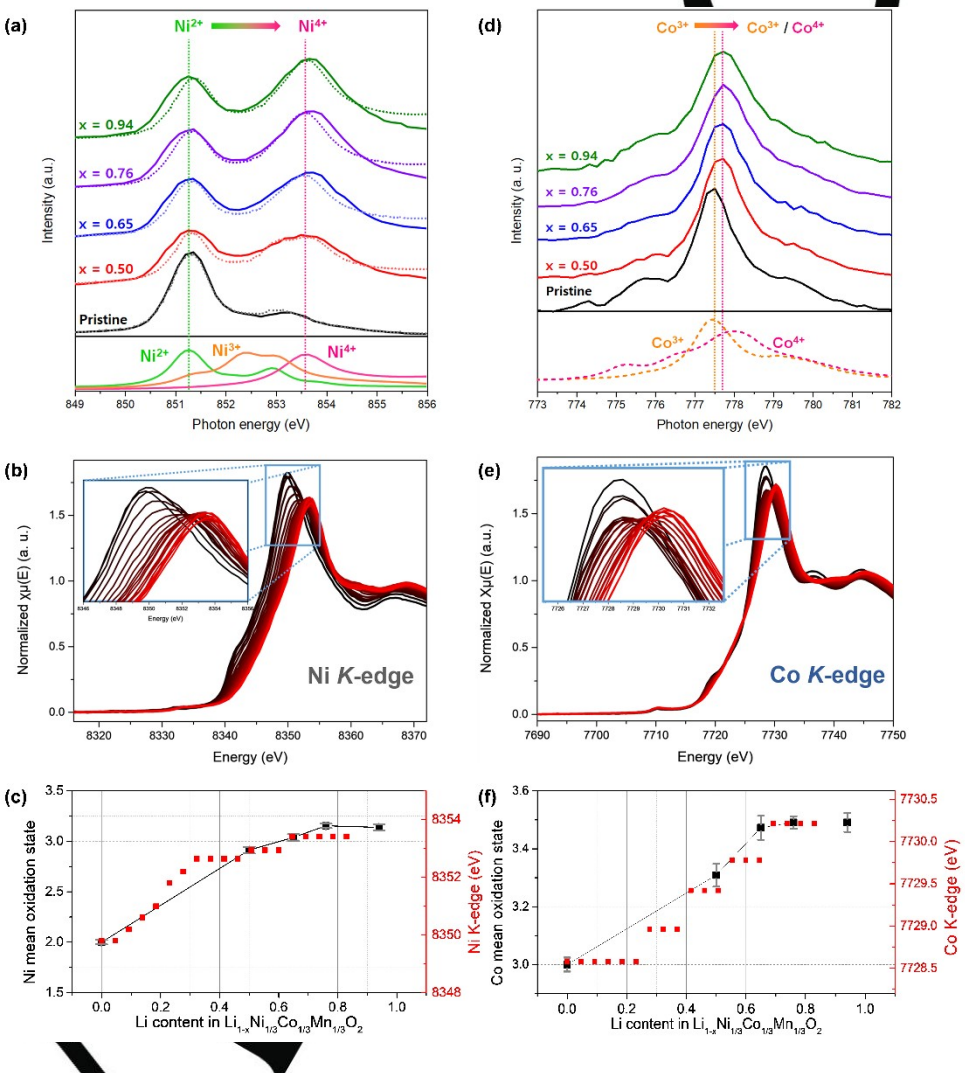

Figure 2. The oxidation state changes of transition metals upon delithiation. (a) sXAS of the Ni L_3-edge collected from a series of electrodes marked as the dots in Figure 1 at different delithiation levels. (b) in-situ hXAS of the Ni *K*-edge, with the shifting leading peak emphasized in the insert. (c) Quantified values of the mean valence states of Ni from sXAS fittings in (a) upon delithiation level (black), consistent with the trend of leading peak shifts of the hXAS results. The quantified value of average Ni valence is presented in Table S3. (d) sXAS results of the Co L_3-edge from the same set of samples (e) in-situ hXAS Co-*K* spectra with the focus on the leading peak shifts in the insert. (f) Quantified mean oxidation state value of Co from sXAS (black) and the trend of leading peak shifts from in-situ hXAS (red).

Figure S1, Table S1 and Supplementary Section 'Powder characterizations of NCM' for more details.) The evaluated charge capacity of NCM is 269 mAh g^{-1}, and its charge behavior shows good accordance with

previous reports about NCM. It was generally believed that, when Li ions are continuously extracted for more than half of its pristine contents, the structural changes and release of oxygen take place and thereby are responsible for the degradation of NCM electrodes. It was also believed that these two detrimental factors are coupled with each other, i.e., oxygen release is associated with the phase change of NCM from layered oxide (MO_2) to spinel (M_3O_4) or rock-salt (MO) at high potentials. Clearly, the key for employing the full theoretical capacity of NCM materials is to utilize the electrochemical capacity at high potentials, where, unfortunately, all these coupled effects take place. Therefore, in this study, we have focused on several specific electrochemical states beyond half delithiation levels with >4.0 V potentials (Colored dots in Figure 1). In this high-voltage range, in addition to the redox states of both the TMs and oxygen, it is equally important to detect the reversibility of the oxygen redox reactions, which is also elaborated by measuring cycled samples in this work.

TM redox reactions

The redox activities of TMs in NCM compounds have been studied before through X-ray absorption spectroscopy.[7b] Here we employ such conventional absorption spectroscopy of both the soft X-ray TM-*L* and hard X-ray TM-*K* edges, with dominating signals from TM 3d and 4p states, respectively, due to the dipole selection rule. Technically, soft X-ray absorption spectroscopy (sXAS) of TM-*L* directly corresponds to the TM-3d valence states, while hard X-ray absorption spectroscopy (hXAS) of TM-*K* benefits from the much deeper probe depth.[8] Although TM-*L* sXAS is a directly TM-3d probe and offers two different probe depth of about 10 nm and 100-200 nm through the electron yield (EY) and fluorescence yield (FY), respectively,[9] the line shape of the bulk-sensitive FY of Mn-*L* are seriously distorted (Figure S2).[10] Therefore, in this work, we also measured Mn-*L* FY signals through inverse partial fluorescence yield (iPFY) extracted from high-efficiency mapping of inelastic X-ray scattering (mRIXS).[11] (See Figure S3, S4 and Supplementary information of "Detailed characterization of NCM through sXAS and mRIXS") The mRIXS-iPFY has been demonstrated to be an effective bulk probe of Mn-*L* without any line-shape distortion for studying battery electrodes.[11] Furthermore, for TM-*L* edges, we have previously established a fitting methodology for quantitative analysis of various TM-*L* sXAS results, allowing us to go beyond previous TM characterization works and obtain quantitative values of the oxidation states of TMs at different electrochemical states.[12] These quantitative analyses are found to be generally consistent with the qualitative results from hXAS, achieving reliable quantitative values of the TM oxidation states in the electrodes. The general consistency between soft and hard XAS results also indicate that the signals of sXAS in the FY and mRIXS-iPFY modes do represent the bulk environment of NCM111.

Figure 2 displays the evolution of the Ni and Co redox states at different electrochemical potentials based on sXAS-FY, and the stable Mn states verified by mRIXS-iPFY (Figure S5). References of different TM states are plotted directly at the bottom of the spectral panels (Figure 2a, 2d and Figure S5) for direct comparisons.[13] The dotted lines in Figure 2a are fittings to the Ni-*L* experimental data by linearly combining the reference spectra calculated through the multiplet theory.[13a] The fitting results display a good match to the experimental data and quantify the Ni oxidation state at each electrochemical state, as shown in Figure 2c. For Co-*L* sXAS, it has been experimentally and theoretically clarified, that the main peak position shifts continuously and linearly from 777.4 eV to 777.9 eV with the valence state changing from 3+ to 4+.[12] Because Co-*L* spectra cannot be fitted by a simple linear combination method due to the flucturation nature of Co states,[12, 13b] the mean valence state of Co is evaluated based on the energy position of the main Co-*L* peak, as displayed in Figure 2f. The detailed value of the Ni and Co mean valence states are summarized in Table S3.

Our quantified TM oxidation state evolution is compared with in-situ hXAS leading peak evolutions shown in Figure 2b and 2e for Ni-*K* and Co-*K*, respectively. We over-plot the energy shifts of the Ni-*K* and Co-*K* in-situ hXAS leading peak in Figure 2c and 2f (red dots). It is clear that the trend of the Ni and Co oxidation state evolution detected by the *K*-edge leading-edge shifts are consistent with the absolute quantification results from sXAS analysis. Based on these quantified values, the total amount of charge transfer from Ni and Co redox centers is calculated, as presented in Table S2 and plotted in Figure 1 (Dashed blue line).

The quantified TM redox reveals the details of the TM evolutions in NCM materials. First, the sXAS of Ni/Co (Figure 2a and 2d) and mRIXS-iPFY of Mn (Figure S5) of the pristine material displays exactly the same line shape as the reference Ni^{2+}, Co^{3+} and Mn^{4+} spectra, thus experimentally concluding the initial TM states in pristine materials as expected $LiNi_{1/3}^{2+}Co_{1/3}^{3+}Mn_{1/3}^{4+}O_2$.[14] Other than the oxidation state, TM-*L* sXAS line shape is also very sensitive to the 3d spin state configurations.[15] The experimental TM-*L* spectra clearly indicate high-spin Ni^{2+}, low-spin $Ni^{3+/4+}$, low-spin $Co^{3+/4+}$ and high-spin $Mn^{2+/3+/4+}$ states (Figure S4 and S6).[12] Second, the evolution of Ni-*L* and Co-*L* line shape upon electrochemical charging clearly shows the systematic oxidation of Ni (Figure 2c) and Co (Figure 2f) while Mn remains unchanged (Figure S5). Again, this quantification is consistent with the hXAS TM-*K* spectral evolution, as discussed above and consistent with previous reports.[7-8]

Third, the quantifications show that both Ni and Co get oxidized up to the 0.65 - 0.74 delithiation range; however, display negligible variation at high potentials (TM redox trend in Figure 1). Such a trend is often taken as the evidence of oxygen redox in literature; however, it is important to note that other irreversible oxidized oxygen, e.g., oxygen release and surface reactions, could also lead to such a trend. Therefore, a direct detection of lattice oxygen redox becomes critical to justify a useful range of reversible oxygen reactions.

Oxygen Activities: TM-O Hybridization and Oxygen Redox Reactions

Our central experimental results on the oxygen activities upon electrochemical cycling through O-*K* mRIXS experiments are displayed in Figure 3. First, O-*K* sXAS results (Figure S7) of a series of electrodes are consistent with previous findings,[7b] the O-*K* pre-edge feature area increases upon charge throughout the cycling process in both the low-voltage and high-voltage regions. It is important to clarify that such an enhancement of O-*K* pre-edge is a common phenomenon for almost all battery electrodes with or without O redox, e.g., $LiFePO_4$.[10, 13a] **The** sXAS **observation** here and in other literatures do not meanshould/could not be used as evidence of **oxygen redox** takes place **throughout the charging process even at low voltages** in NCM or other materials,; **instead, it only indicates a** much **enhanced TM-O hybridization** upon charging, which that **dominates** this the **O-*K* pre-edge intensity** and lineshape,[11] .[10] We note that this has long been studied and known in physics,which actually has been studied and confirmed both theoretically and experimentally in physics field.[16] and our latest analysis shows that the evolution of O-K sXAS pre-edge in oxide based battery electrodes is almost completely controled by TM states, not oxygen[17] . Nonetheless, the clear O-*K* sXAS pre-edge features in all samples indicate a strong TM-O hybridization throughout the electrochemical process.

We have recently demonstrated that, through the new dimension on the fluorescence photon energy,

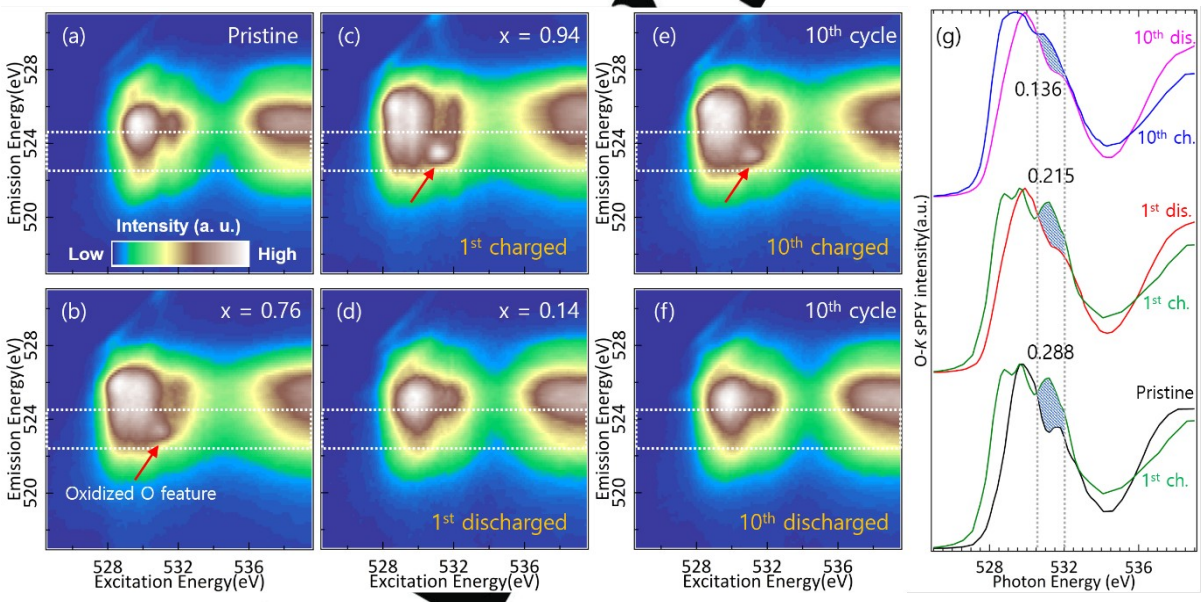

Figure 3. O oxidation behaviors during the charging process. (a-d) O-*K* mRIXS of different SOCs during the 1st cycle, where the oxidized oxygen feature (highlighted by red arrows) emerges at x = 0.76 (b), enhances at fully charged (c) and disappear at fully discharged (d), indicating the occurrence of a reversible anionic redox in NMC. O-*K* mRIXS of the 10th fully charged and discharged. The oxygen redox is still clear although the intensity drops. (g) O-*K* sPFY extracted by integrating the intensity within the characteristic emission-energy range from 522.5 eV to 524.5 eV on the O-*K* mRIXS (white dotted boxes). The numbers represent the shaded area between the charged and discharged/pristine electrodes, which is the quantified value of the intensity variation of the oxidized oxygen feature in O-*K* mRIXS. The ratio of these numbers provide the estimation of the initial cycle reversibility (0.215/0.288 = 75%) and the capacity retention after 10 cycles (0.136/0.215 = 63%) of the oxygen redox reactions. The mRIXS results and mRIXS-sPFY analysis of the full set of electrodes are presented in Figure S7 and Table S2, which is visualized in Figure 4.

In order to uncover the intrinsic lattice oxygen redox activities, we employed the recently demonstrated high-effeciency mRIXS technique,[18] which has quickly been recognized as the tool-of-choice for detecting the lattice (non-released) oxidized oxygen in battery electrodes.[10-11] Particularly,called emission energy, provided in mRIXS results, a specific feature at emission energy of around 523.7 eV and excitation energy of around 531 eV

fingerprints the oxidized oxygen state,[19] which could be clearly distinguished from the strong TM-O hybridization signals at emission energy of 525 eV. Such a feature ~~fingerprint could therefore serve a~~is a reliable probe of the oxygen redox activities in the lattice, which has been verified in many Li-ion and Na-ion systems by this time.[10-11] As an additional note, we have a very recent ~~shown that paper by Radin etc., questions the validity of the mRIXS findings based on our reports of radiation damage effect of $LiAlO_2$,[20] which shows that radiation introduces the oxidized oxygen feature.[21] As a matter of fact, we have already shown in the same work that~~ the oxidized oxygen mRIXS feature in battery electrodes will be eliminated by radiation effect, instead of being introduced,[20] which directly rules out the possibility of photon-induced mRIXS feature of oxidized oxygen. The mRIXS observation of the oxidized oxygen in the electrode lattice is thus intrinsic.[20]

Figure 3 displays the mRIXS results of the key electrodes during the initial and the 10th cycle at different electrochemical states. Figure S8 shows the mRIXS results of more samples that we measured. The very broad and dominating features around 522-527 eV emission energy (vertical axis) are typical signals from conventional O^{2-} states.[21] The signals below 535 eV excitation energy (horizontal axis) correspond directly to the pre-edge features in sXAS from TM-O hybridization. mRIXS shows that these features are broadened and enhanced during charging even with x below 0.65, indicating an enhanced TM-O hybridization throughout the electrochemical range, as discussed above. The broad features above 535 eV excitation energy are from the hybridization to the TM 4s/4p states and the itinerant ~~O 3p~~ oxygen bands at high energies.[21]

Strikingly, a dedicated sharp feature at 523.7 eV emerges at (only) high voltages with the delithiation level (x) above 0.65 (Figure 3, Figure S8e), representing the true signals of oxidized oxygen in the lattice.[10-11] Furthermore, Figure 3 shows that this feature gets enhanced upon charging and reaches its strongest form in a fully charged state (x = 0.94). More importantly, after discharge, this feature completely disappears, indicating a reversible reduction process, i.e., oxygen redox. We also show that, after 10 cycles, although the oxygen redox feature gets weakened in general, it could still be observed clearly in the charged NCM electrode and displays a reversible reduction reaction upon discharge (Figure 3e and 3f). Because the appearance and disappearance of the specific oxygen redox feature in mRIXS correspond to the oxidation and reduction states of the oxygen, the reversibility of the lattice oxygen redox reactions could be estimated by following the intensity change upon cycling.[11] This analysis could be easily achieved by extracting the mRIXS intensity within the interested emission energy range (white rectangular in Figure 3), the so-called super partial fluorescence yields (sPFY).[11] Figure 3g and Figure S8e display the sPFY spectra obtained by integrating the intensity within 522.5 to 524.5 eV emission energy range of mRIXS. The intensity evolution of the oxygen redox feature at 530.5 to 532

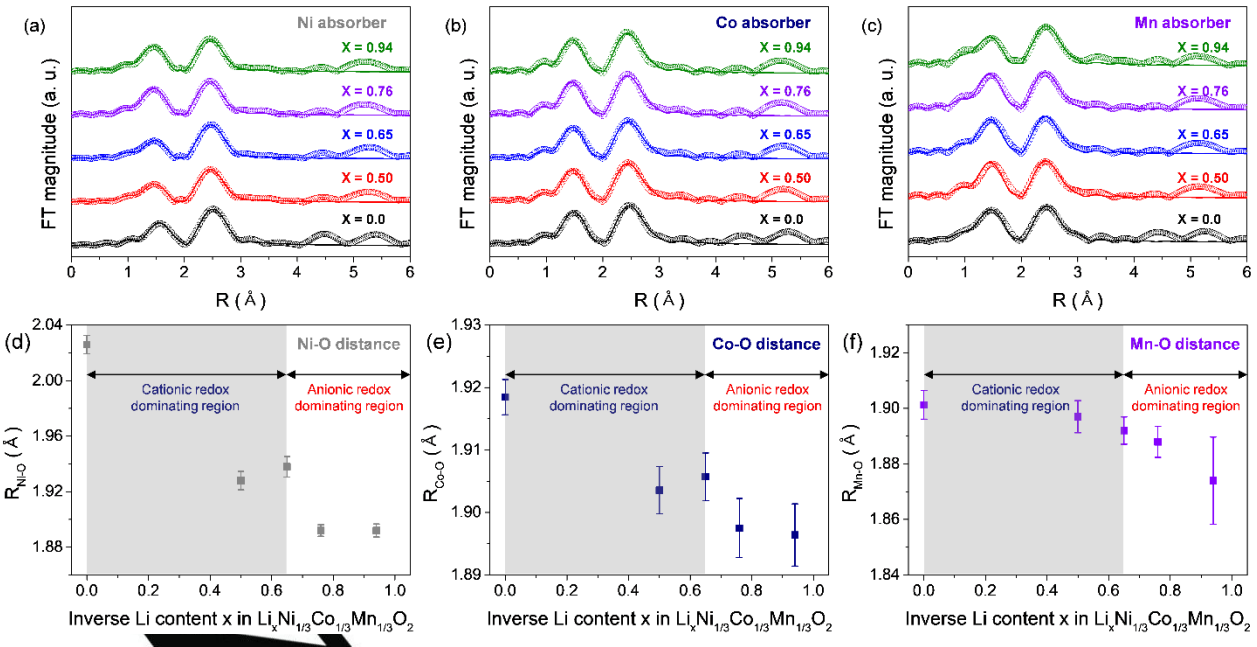

Figure 4. Ex-situ EXAFS analyses during charge. Fourier transformed spectra of the extended edge spectra of Ni-*K* (a), Co-*K* (b) and Mn-*K* (c) upon delithiation level (x) in $Li_{1-x}Ni_{1/3}Co_{1/3}Mn_{1/3}O_2$ (NCM). TM-O Bonding distances are fitted from the first shell of Ni-O (d), Co-O (e) and Mn-O (f) as a function of the delithiation level.

eV excitation energy range (shaded in Figure 3g and S8e) are summarized in Table S2 and illustrated in Figure 1 (red line).

Therefore, the mRIXS results and sPFY quantification reveal that reversible lattice oxygen redox reactions take place when the system is more than half delithiated. More importantly, such an oxygen redox reaction in conventional NCM material is reversible and could be clearly seen after cycling. For quantifying the reversbility of oxygen redox, all the sPFY spectra were normalized to the hybridization peak at 529.7 eV so that the relative intensity at 531.0 eV could be compared at different eletrochemical states. Though the normalization will always affect the absolute intensity, however, only relative intensity change between charged and discharged states are concerned. Figure 3g displays the relative intensity variation of the specific oxygen redox feature in sPFY, with the shaded area representing the differences in the amount of oxidized oxygen between the charged and discharged states, during the 1st charging (0.288), 1st discharging (0.215), and the 10th discharging (0.136) cycles. The ratio of the area change suggests the first-cycle reversibility and the 10-cycle capacity retention of the oxygen redox,[11] about 75% (0.215/0.288) reversibility during the initial charge/discharge, and a retention of about 63% (0.136/0.215) after 10 cycles. Therefore, while TM-O hybridization is strong throughout the whole potential range and gets enhanced during charging, the intrinsic lattice oxygen redox reactions only take place in highly (X > 0.5) delithiated states. It is also remarkable that mRIXS technique characterizes the oxygen redox reaction in a conventional NCM system with a decent reversibility, i.e., 75% first cycle reversibility and 63% retention after 10 cycles. It is worthy noting that the quantification of O redox from mRIXS-~~iPFY~~ sPFY analysis is applicable on many other battery elelctrode systems, including $Na_{2/3}Mg_{1/3}Mn_{2/3}O_2$ and Li-rich $Li_{1.17}Ni_{0.21}Co_{0.08}Mn_{0.54}O_2$.[11] While the mRIXS-sPFY lineshape is highly material dependent because of the strong background signals from TM-O hybridization effect, it provides an unique opportunity to distinguish~~For materials with other oxygen reactions, especially oxygen release, the quantification through mRIXS-sPFY quantifies~~ the lattice oxygen redox contributions from other irreversible oxygen activities.[22] ~~, i.e., only the "good" part of the oxidized oxygen, indicating the material-dependence of the quantification methods.~~

To get the insight of the local environment associated with the oxygen framework, we conducted the hard X-ray extended absorption fine structure (EXAFS) analysis to identify the local structure change of MO_6. The elemental sensitivity of the EXAFS enables the findings on which configuration plays the key role in the oxygen redox reactions. Figure 4 shows the EXAFS spectra obtained through Fourier transformation (FT) for the NCM electrode, and the fitted parameters for FT spectra have suggested in Table S4-S6. The first FT peak is attributed to the bonding distance between M and O in all absorbers and shows the peak shift to shorter inter-atomic distance as Li content decreases. The second peak represents the second shell M-M distance. All the bonding lengths of the first shell of M-O (Figure 4d-f) and second shell of M-M (Figure S9) were investigated specifically with the delithiation level (x). For both the Ni-O and Co-O bonding length, the values decreases with x. The decrease with x < 0.65 is due to the shrinkage of Ni and Co ionic radius resulting from their oxidation (Figure 3 and 2). However, although no further oxidation is found beyond x > 0.65 (Figure 1 and 2), the Ni-O and Co-O bonding length is continuously reduced to ~ 1.890 Å for Ni-O and 1.895 Å for Co-O at x = 0.94, indicating the oxidation of O around Ni and Co. In contrast, for Mn-O bond length, while the negligible reduction with x < 0.65 is expected due to the unchanged Mn^{4+}, the obvious decrease of Mn-O bond length is only observed at highly delithiated levels with x > 0.8, where the Ni-O and Co-O seems stable. Additionally, the variation of the M-M distance is more or less the same for all TMs, as shown in Figure S9. The different behaviors of the first peak (M-O) and second peak (M-M) could be natually understood if one considers that the M-M distance is strongly affected by the M-O bond length due to the edge-shared octahydral structure. Therefore, the variation of the M-O in Figure 4d-f represents the intrinsic local structural change, which also affects the M-M distance with an overall averaged (same) trend. The interesting contrast between the Mn-O and Ni/Co-O strongly suggests that TM environment plays a critical role in the oxygen redox reactions. Naively, we could speculate that oxygen is activated in the vicinity of Ni/Co when the delithiation level is more than half, but oxygen becomes oxidized around Mn only at very high delithiation level. This also triggers another critical question on whether the types of oxygen oxidations are different between Mn and Ni/Co. Considering that irreversible behaviors are often observed at very high potentials, the strong Mn-O variation at the highly delithated levels may indicate specific irreversible oxygen activities if the cluster of Mn^{4+}-O were further oxidized. Such a TM dependence on oxygen redox reactions could also be different in different material systems. The answers to all these questions are crucial for an ultimate understanding of the oxygen redox reactions in battery electrodes, and we expect the combined and direct experimental evidences here will inspire many future experimental and theoretical studies.

In summary, we provide so far the most direct, reliable and detailed experimental analysis of the redox mechanism on both the cationic and anionic activities across the full cycling range of conventional NCM materials. Reversible lattice oxygen redox reactions at high potentials are clearly revealed. The transition metal

redox activity from Ni^{2+}/Ni^{4+} and Co^{3+}/Co^{4+} dominates the charge compensation with the delithiation level x < 0.65. The oxygen involvement through TM-O hybridization is enhanced upon charging and is strong throughout the whole potential range. Importantly, the further delithiation above x = 0.65 predominantly depends on the dedicated anionic redox activity, which contributes to the excess capacity at the high potential range. While mRIXS detects only the lattice oxygen redox reactions, increasing charging potential often lead to irreversible O loss and associated surface reactions. This is evidenced by the 63% retention rate after only 10 cycles as extracted in this work. Indeed, if the O redox reaction was extended to 4.8 V vs. Li/Li^+, a large irreversible capacity coming up to 40 mAh g^{-1} was observed during the following discharge. Moreover, cyclic degradation in ~ 0.76 < x < ~ 0.94 region also suggests that the highly oxidized states need to be further understood and carefully controlled (Figure S10). Nevertheless, our work shows that O redox activity could be reversible in conventional NCM systems. Such a possibility is essential for breaking the capacity limitation of the layered conventional compound. Additionally, the ~ 0.67 < x < ~ 0.76 region also triggers the O redox, however exhibits a stable cycle performance (Figure S10). Such a clarification provides the optimism for breakthroughs in the capacity of non-overlithiated layered oxides. Fundamentally, the combined soft and hard X-ray results suggest that TMs play a critical role in determining the oxygen activities, which could be the reason for the improved oxygen redox stability by replacing 3d transition metals with other heavy transition metals with a trade-off in cost.

Conclusion

There have been a lot of debates about the oxygen redox in the Ni-based layered oxide materials in the past 20 years. In this work, w**We have investigated the redox chemistry of** conventional **NCM** electrode across a wide voltage range through state-of-the-art spectroscopic characterizations of both the cationic and anionic states. , and t**The** reversible **anionic redox activity** was is unambeduously revealedproved **by mRIXS** in the consistency with previous XAS results. **The results also provide detailed information about the contribution of TM and oxygen in charge compensation of NCM** at different potential range through their quantification that enables to establish a proper strategy for stabilization of materials, which suggests two kinds of oxygen activities involved in NCM cycling: the TM-O hybridization throughout the whole cycling range and the lattice oxygen redox only at high potentials. Again, o**Our results raise** lots of **critical questions** regarding the oxygen redox reactions as discussed above, and and we expect many future efforts triggered by the findings here, which will lead to both the fundamental clarifications of the reaction mechanism and the material optimizations towards a maximized energy density in non-overlithiated layered compounds, e.g., such as $LiNi_{1-x-y}Co_xMn_yO_2$.

Acknowledgements

Y.-M. K.ang acknowledges that this work was supported by the National Research Foundation of Korea (NRF) grant funded by the Korea government (MSIP) (NRF-2017R1A2B3004383). M. Cho acknowledges the financial supportfrom a National Research Foundation of Korea (NRF) grant funded by the Korean government (MSIP) (2012R1A1A2048841). Soft X-ray experiments were performaed at BL8.0.1 of The the Advanced Light Source (ALS) is, a DOE Office of Science User Facility under contract no. DE-AC02-05CH11231. G.-H.L. and J.W. acknowledge the financial support from ALS fellowship program.

Keywords: • Electrochemistry • Mapping of resonant inelastic X-ray scattering (mRIXS) • Lithium ion batteries • Redox chemistry • X-ray absorption spectroscopy

[1] aA. S. Arico, P. Bruce, B. Scrosati, J. M. Tarascon, W. van Schalkwijk, *Nat. Mater.* **2005**, *4*, 366-377; bM. Armand, J. M. Tarascon, *Nature* **2008**, *451*, 652-657; cJ. B. Goodenough, K. S. Park, *J. Am. Chem. Soc.* **2013**, *135*, 1167-1176; dD. W. Han, S. J. Lim, Y. I. Kim, S. H. Kang, Y. C. Lee, Y. M. Kang, *Chem. Mat.* **2014**, *26*, 3644-3650; eM. S. Islam, C. A. Fisher, *Chem. Soc. Rev.* **2014**, *43*, 185-204; fM. R. Jo, Y. I. Kim, Y. Kim, J. S. Chae, K. C. Roh, W. S. Yoon, Y. M. Kang, *ChemSusChem* **2014**, *7*, 2248-2254; gS.-W. Kim, D.-H. Seo, X. Ma, G. Ceder, K. Kang, *Adv. Energy Mater.* **2012**, *2*, 710-721; hJ. Shin, J. Yang, C. Sergey, M. S. Song, Y. M. Kang, *Adv. Sci.* **2017**, *4*, 1700128-1700136; iJ. M. Tarascon, M. Armand, *Nature* **2001**, *414*, 359-367; jJ. Yang, D. W. Han, M. R. Jo, K. Song, Y. I. Kim, S. L. Chou, H. K. Liu, Y. M. Kang, *J. Mater. Chem. A* **2015**, *3*, 1005-1009; kJ. Yang, S. Muhammad, M. R. Jo, H. Kim, K. Song, D. A. Agyeman, Y. I. Kim, W.

S. Yoon, Y. M. Kang, *Chem. Soc. Rev.* **2016**, *45*, 5717-5770.

[2] S. H. Min, M. R. Jo, S.-Y. Choi, Y.-I. Kim, Y.-M. Kang, *Adv. Energy Mater.* **2016**, *6*, 1501717-1501729.

[3] aZ. Chen, J. Wang, D. Chao, T. Baikie, L. Bai, S. Chen, Y. Zhao, T. C. Sum, J. Lin, Z. Shen, *Sci. Rep.* **2016**, *6*, 25771-25780; bJ.-Y. Hwang, C. S. Yoon, I. Belharouak, Y.-K. Sun, *J. Mater. Chem. A* **2016**, *4*, 17952-17959; cS.-H. Kang, J. Kim, M. E. Stoll, D. Abraham, Y.-K. Sun, K. Amine, *J. Power Sources* **2002**, *112*, 41-48; dH. Kim, M. G. Kim, H. Y. Jeong, H. Nam, J. Cho, *Nano Lett* **2015**, *15*, 2111-2119; eL. Li, L. Wang, X. Zhang, M. Xie, F. Wu, R. Chen, *ACS Appl. Mater. Interfaces* **2015**, *7*, 21939-21947; fJ. M. Lim, T. Hwang, D. Kim, M. S. Park, K. Cho, M. Cho, *Sci. Rep.* **2017**, *7*, 39669-39678; gC. Venkateswara Rao, A. Leela Mohana Reddy, Y. Ishikawa, P. M. Ajayan, *ACS Appl. Mater. Interfaces* **2011**, *3*, 2966-2972.

[4] aC. Delmas, *Nat. Chem.* **2016**, *8*, 641-643; bK. Luo, M. R. Roberts, R. Hao, N. Guerrini, D. M. Pickup, Y. S. Liu, K. Edstrom, J. Guo, A. V. Chadwick, L. C. Duda, P. G. Bruce, *Nat. Chem.* **2016**, *8*, 684-691; cE. McCalla, A. M. Abakumov, M. Saubanère, D. Foix, E. J. Berg, G. Rousse, M.-L. Doublet, D. Gonbeau, P. Novák, G. Van Tendeloo, R. Dominko, J.-M. Tarascon, *Science* **2015**, *350*, 1516-1521; dB. Mortemard de Boisse, G. Liu, J. Ma, S. Nishimura, S. C. Chung, H. Kiuchi, Y. Harada, J. Kikkawa, Y. Kobayashi, M. Okubo, A. Yamada, *Nat. Commun.* **2016**, *7*, 11397-11405; eP. E. Pearce, A. J. Perez, G. Rousse, M. Saubanère, D. Batuk, D. Foix, E. McCalla, A. M. Abakumov, G. Van Tendeloo, M. L. Doublet, J. M. Tarascon, *Nat. Mater.* **2017**, *16*, 580-587; fP. Rozier, M. Sathiya, A.-R. Paulraj, D. Foix, T. Desaunay, P.-L. Taberna, P. Simon, J.-M. Tarascon, *Electrochem. Commun.* **2015**, *53*, 29-32; gM. Sathiya, G. Rousse, K. Ramesha, C. P. Laisa, H. Vezin, M. T. Sougrati, M. L. Doublet, D. Foix, D. Gonbeau, W. Walker, A. S. Prakash, M. Ben Hassine, L. Dupont, J. M. Tarascon, *Nat. Mater.* **2013**, *12*, 827-835; hM. Saubanère, E. McCalla, J. M. Tarascon, M. L. Doublet, *Energy Environ. Sci.* **2016**, *9*, 984-991; iD. H. Seo, J. Lee, A. Urban, R. Malik, S. Kang, G. Ceder, *Nat. Chem.* **2016**, *8*, 692-697; jY. Xie, M. Saubanère, M. L. Doublet, *Energy Environ. Sci.* **2017**, *10*, 266-274; kN. Yabuuchi, M. Nakayama, M. Takeuchi, S. Komaba, Y. Hashimoto, T. Mukai, H. Shiiba, K. Sato, Y. Kobayashi, A. Nakao, M. Yonemura, K. Yamanaka, K. Mitsuhara, T. Ohta, *Nat. Commun.* **2016**, *7*, 13814-13823.

[5] J. R. Croy, M. Balasubramanian, K. G. Gallagher, A. K. Burrell, *Acc. Chem. Res.* **2015**, *48*, 2813-2821.

[6] aC.-H. Chen, B.-J. Hwang, C.-Y. Chen, S.-K. Hu, J.-M. Chen, H.-S. Sheu, J.-F. Lee, *J. Power Sources* **2007**, *174*, 938-943; bL. Dahéron, R. Dedryvère, H. Martinez, M. Ménétrier, C. Denage, C. Delmas, D. Gonbeau, *Chem. Mat.* **2008**, *20*, 583-590.

[7] aY. W. Tsai, B. J. Hwang, G. Ceder, H. S. Sheu, D. G. Liu, J. F. Lee, *Chem. Mat.* **2005**, *17*, 3191-3199; bW. S. Yoon, M. Balasubramanian, K. Y. Chung, X. Q. Yang, J. McBreen, C. P. Grey, D. A. Fischer, *J. Am. Chem. Soc.* **2005**, *127*, 17479-17487.

[8] aA. Deb, U. Bergmann, S. P. Cramer, E. J. Cairns, *J. Appl. Phys.*

2005, *97*, 113523-113533; bB. J. Hwang, Y. W. Tsai, D. Carlier, G. Ceder, *Chem. Mat.* **2003**, *15*, 3676-3682; cD. Buchholz, J. Li, S. Passerini, G. Aquilanti, D. Wang, M. Giorgetti, *ChemElectroChem* **2015**, *2*, 85-97.

[9] W. Yang, X. Liu, R. Qiao, P. Olalde-Velasco, J. D. Spear, L. Roseguo, J. X. Pepper, Y.-d. Chuang, J. D. Denlinger, Z. Hussain, *J. Electron Spectrosc.* **2013**, *190*, 64-74.

[10] W. Yang, T. P. Devereaux, *J. Power Sources* **2018**, *389*, 188-197.

[11] K. Dai, J. Wu, Z. Zhuo, Q. Li, S. Sallis, J. Mao, G. Ai, C. Sun, Z. Li, W. E. Gent, W. C. Chueh, Y.-d. Chuang, R. Zeng, Z.-x. Shen, F. Pan, S. Yan, L. F. J. Piper, Z. Hussain, G. Liu, W. Yang, *Joule* **2019**, *3*, 518-541.

[12] Q. Li, R. Qiao, L. A. Wray, J. Chen, Z. Zhuo, Y. Chen, S. Yan, F. Pan, Z. Hussain, W. Yang, *J. Phys. D* **2016**, *49*, 413003.

[13] aX. Liu, Y. J. Wang, B. Barbiellini, H. Hafiz, S. Basak, J. Liu, T. Richardson, G. Shu, F. Chou, T. C. Weng, D. Nordlund, D. Sokaras, B. Moritz, T. P. Devereaux, R. Qiao, Y. D. Chuang, A. Bansil, Z. Hussain, W. Yang, *Phys. Chem. Chem. Phys.* **2015**, *17*, 26369-26377; bR. Qiao, J. Liu, K. Kourtakis, M. G. Roelofs, D. L. Peterson, J. P. Duff, D. T. Deibler, L. A. Wray, W. Yang, *J. Power Sources* **2017**, *360*, 294-300.

[14] aZ. Li, N. A. Chernova, M. S. Whittingham, F. M. Alamgir, *J. Mater. Chem.* **2012**, *22*, 19993-20000; bW.-S. Yoon, K.-B. Kim, M.-G. Kim, M.-K. Lee, H.-J. Shin, J.-M. Lee, J.-S. Lee, C.-H. Yo, *J. Phys. Chem. B* **2002**, *106*, 2526-2532.

[15] J. Wu, J. Song, K. Dai, Z. Zhuo, L. A. Wray, G. Liu, Z. X. Shen, R. Zeng, Y. Lu, W. Yang, *J. Am. Chem. Soc.* **2017**, *139*, 18358-18364.

[16] aF. M. de Groot, M. Grioni, J. C. Fuggle, J. Ghijsen, G. A. Sawatzky, H. Petersen, *Phys. Rev. B* **1989**, *40*, 5715-5723; bP. Olalde-Velasco, J. Jiménez-Mier, J. Denlinger, W. L. Yang, *Phys. Rev. B* **2013**, *87*; cP. Olalde-Velasco, J. Jiménez-Mier, J. D. Denlinger, Z. Hussain, W. L. Yang, *Phys. Rev. B* **2011**, *83*; dJ. Zaanen, G. A. Sawatzky, J. W. Allen, *Phys. Rev. Lett.* **1985**, *55*, 418-421.

[17] R. Qiao, S. Roychoudhury, Z. Zhuo, Q. Li, Y. Lyu, J.-H. Kim, J. Liu, F. Lee, B. J. Polzin, J. Guo, S. Yan, Y. Hu, H. Li, D. Prendergast, W. Yang, *ChemRxiv. Preprint.* *https://doi.org/10.26434/chemrxiv.11416374.v2* **2019**.

[18] R. Qiao, Q. Li, Z. Zhuo, S. Sallis, O. Fuchs, M. Blum, LotharWeinhardt, C. Heske, J. Pepper, M. Jones, A. Brown, A. Spucces, K. Chow, B. Smith, P.-A. Glans, Y. Chen, S. Yan, F. Pan, L. F. J. Piper, J. Denlinger, J. Guo, Z. Hussain, Y.-D. Chuang, W. Yang, *Review of Scientific Instruments* **2017**, *88*, 033106.

[19] aZ. Zhuo, C. D. Pemmaraju, J. Vinson, C. Jia, B. Moritz, I. Lee, S. Sallies, Q. Li, J. Wu, K. Dai, Y. D. Chuang, Z. Hussain, F. Pan, T. P. Devereaux, W. Yang, *J. Phys. Chem. Lett.* **2018**, *9*, 6378-6384; bZ. Zhuo, Y.-s. Liu, J. Guo, Y.-d. Chuang, F. Pan, W. Yang, *ChemRxiv. Preprint.* *https://doi.org/10.26434/chemrxiv.11340170.v1* **2019**.

[20] Z. W. Lebens-Higgins, J. Vinckeviciute, W. J., N. V. Faenza, Y. Li, S. Sallis, N. Pereira, Y. S. Meng, G. G. Amatucci, A. Van der Ven, W. Yang, L. F. J. Piper, *J. Phys. Chem. C* **2019**, *123*, 13201-13207.

[21] S. M. Butorin, J. Guo, N. Wassdahl, E. J. Nordgren, *J. Electron Spectrosc.* **2000**, *110-111*, 235-273.

[22] J. Wu, Z. Zhuo, X. Rong, K. Dai, Z. Lebens-Higgins, S. Sallis, F. Pan, L. F. J. Piper, G. Liu, Y.-d. Chuang, Z. Hussain, Q. Li, R. Zeng, Z.-x. Shen, W. Yang, *Science Advances* **2020**, *In Press*.

Entry for the Table of Contents

RESEARCH ARTICLE

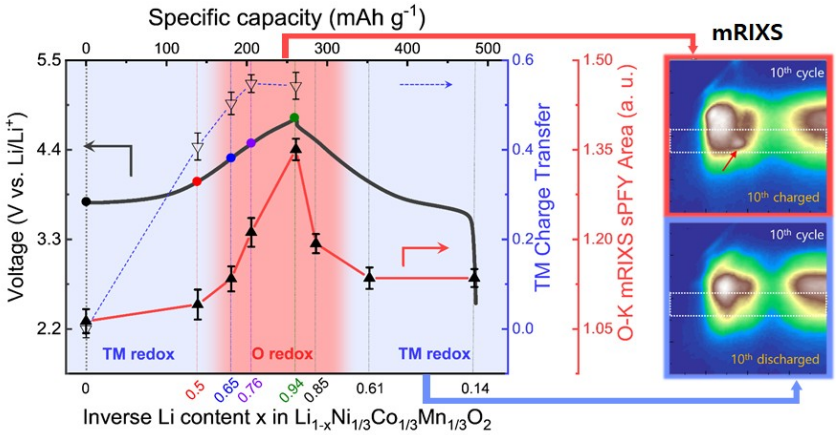

Gi-Hyeok Lee, Jinpeng Wu, Duho Kim, Kyeongjae Cho, Maenghyo Cho, Wanli Yang, Yong-Mook Kang

Page No. – Page No.

Reversible Anionic Redox Activities in Conventional $LiNi_{1/3}Co_{1/3}Mn_{1/3}O_2$ Cathodes

Reversible anionic redox activities in $LiNi_{1/3}Co_{1/3}Mn_{1/3}O_2$ have experimentally proved by synchrotron techniques including mRIXS which is a state-of-the-art characterization. The unique feature of the RIXS map indicates that the anionic redox is evolved in high voltage region, and the two redox behaviours, cationic and anionic redox, of $LiNi_{1/3}Co_{1/3}Mn_{1/3}O_2$ have been investigated in detail by quantification of redox.